NRC·CNRC

NRC Publications Archive
Archives des publications du CNRC

High-frequency torsional motion transduction using optomechanical coupled oscillators

Kaviani, Hamidreza; Behera, Bishnupada; Hajisalem, Ghazal; Luiz, Gustavo de Oliveira; Lake, David P.; Barclay, Paul E.

This publication could be one of several versions: author's original, accepted manuscript or the publisher's version. / La version de cette publication peut être l'une des suivantes : la version prépublication de l'auteur, la version acceptée du manuscrit ou la version de l'éditeur.
For the publisher's version, please access the DOI link below./ Pour consulter la version de l'éditeur, utilisez le lien DOI ci-dessous.

Publisher's version / Version de l'éditeur:
https://doi.org/10.1364/OPTICA.473187
Optica, 10, 1, pp. 35-41, 2023-01-05

NRC Publications Archive Record / Notice des Archives des publications du CNRC :
https://nrc-publications.canada.ca/eng/view/object/?id=59220ce8-97b7-4a85-918d-0a4aa4309ef2
https://publications-cnrc.canada.ca/fra/voir/objet/?id=59220ce8-97b7-4a85-918d-0a4aa4309ef2

Access and use of this website and the material on it are subject to the Terms and Conditions set forth at
https://nrc-publications.canada.ca/eng/copyright
READ THESE TERMS AND CONDITIONS CAREFULLY BEFORE USING THIS WEBSITE.

L'accès à ce site Web et l'utilisation de son contenu sont assujettis aux conditions présentées dans le site
https://publications-cnrc.canada.ca/fra/droits
LISEZ CES CONDITIONS ATTENTIVEMENT AVANT D'UTILISER CE SITE WEB.

Questions? Contact the NRC Publications Archive team at PublicationsArchive-ArchivesPublications@nrc-cnrc.gc.ca. If you wish to email the authors directly, please see the first page of the publication for their contact information.

Vous avez des questions? Nous pouvons vous aider. Pour communiquer directement avec un auteur, consultez la première page de la revue dans laquelle son article a été publié afin de trouver ses coordonnées. Si vous n'arrivez pas à les repérer, communiquez avec nous à PublicationsArchive-ArchivesPublications@nrc-cnrc.gc.ca.

National Research Council Canada | Conseil national de recherches Canada

Canada

Research Article Vol. 10, No. 1 / January 2023 / Optica 35

OPTICA

High-frequency torsional motion transduction using optomechanical coupled oscillators

Hamidreza Kaviani,[1,2,†] Bishnupada Behera,[1,2,†] Ghazal Hajisalem,[1,2] Gustavo de Oliveira Luiz,[3] David P. Lake,[1,2] and Paul E. Barclay[1,2,*]

[1]Institute for Quantum Science and Technology, University of Calgary, Calgary, Alberta, T2N 1N4, Canada
[2]National Research Council of Canada Nanotechnology Research Centre, Edmonton, Alberta, T6G 2M9, Canada
[3]nanoFAB Centre, University of Alberta, Edmonton, Alberta, T6G 2V4, Canada
*Corresponding author: pbarclay@ucalgary.ca

Received 15 August 2022; revised 10 October 2022; accepted 11 November 2022; published 5 January 2023

Using light to measure an object's motion is central to operating mechanical sensors that probe forces and fields. Cavity optomechanical systems embed mechanical resonators inside optical resonators. This enhances the sensitivity of optomechanical measurements, but only if the mechanical resonator does not spoil the properties of the optical cavity. For example, cavity optomechanical detection of resonators made from optically absorbing materials, or whose geometry does not possess suitable spatial symmetry, is challenging. Here we demonstrate a system that overcomes challenges in measuring high-frequency twisting motion of a nanodisk by converting them to vibrations of a photonic crystal cavity. Optomechanical readout of the cavity then enables measurement of the nanodisk's torsional resonances with sensitivity $5.1 \times 10^{-21} - 1.2 \times 10^{-19}$ Nm/$\sqrt{\text{Hz}}$ for a mechanical frequency range of 5–800 MHz. The nanodisk can be outfitted with magnetic nanostructures or metasurfaces without affecting the optical properties of the cavity, making the system suitable for torque magnetometry and structured light sensing. © 2023 Optica Publishing Group under the terms of the Optica Open Access Publishing Agreement

https://doi.org/10.1364/OPTICA.473187

1. INTRODUCTION

The enhanced optomechanical interaction between light and mechanical resonances in nanophotonic cavities allows ultra-precise measurement of force and displacement [1–9], enabling sensors including accelerometers [10], ultrasound detectors [11], mass spectrometers [12,13], and atomic force measurement devices [14]. Cavity optomechanical devices can also sensitively detect torque [15–19], leading to advances in torque magnetometry [20,21], spin detection of electrons [22], and measurement of photon spin and orbital angular momentum [17,19]. Ideally, mechanical resonators in these systems are integrated directly within the optical cavity to maximize transduction strength: the conversion of mechanical motion to an optical response. However, many of these applications require metallic or magnetic materials that degrade the cavity's properties if they interact with its optical field. For example, torque magnetometers incorporate permalloy nanostructures [20], while mechanical transducers of microwave fields incorporate metal [23]. Challenges also arise with resonators whose geometry precludes their integration directly within nanoscale cavities such as photonic crystals and whispering gallery mode resonators whose optical confinement relies upon precisely engineered geometry that cannot be perturbed, or whose mechanical resonance spatial symmetry results in vanishing optomechanical coupling to a cavity's optical field.

Previously, these challenges have been addressed using mechanical resonators whose interaction with the cavity optical field is limited to regions not patterned with lossy material [20], or with resonators that only weakly perturb the optical cavity volume [21], enabling sensitive transduction of megahertz frequency mechanical resonances. Here we demonstrate a new approach that couples two mechanical resonators—one actuated by an external signal, and one integrated within an optical cavity—allowing individual optimization of the system's actuation and readout properties. We show that through resonant mechanical coupling, a photonic crystal readout cavity can sensitively monitor motion of a high mechanical frequency nanodisk positioned far from the cavity's optical mode. The nanodisk's resonances are suited for actuation by sources of torque commonly encountered in magnetometry [20] and structured light [19], and can be designed to reach frequencies >700 MHz, nearly two orders of magnitude larger than previous optomechanical torque sensors [20,22]. The photonic crystal cavity allows sensitive measurement of the nanodisks's mechanical resonances via their resonant mechanical coupling to its mechanical modes. This enables the detection of high-frequency nanodisk modes, creating a path towards resonant measurement of nanomagnetic dynamics [24], enhancement of the Einstein–de Haas effect [25,26], studies of spin and orbital angular momentum of photons and electrons [19,22,27], and transduction of radiofrequency signals [24,28,29].

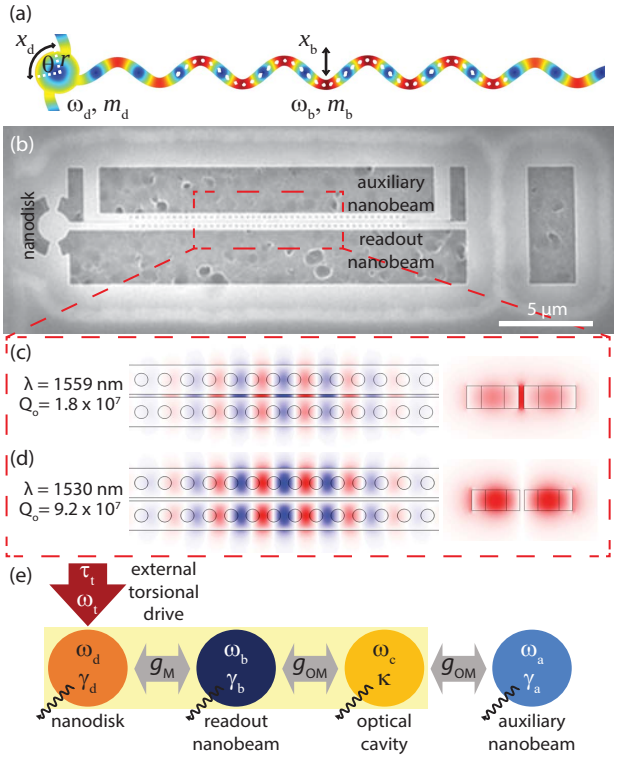

Fig. 1. (a) Finite element simulation of an in-plane hybridized torsional resonance of the device. Note that the nanodisk's displacement x_d is related to the radius r and angle of rotation θ of the nanodisk by $x_d = r\theta$, using the small angle approximation. (b) SEM image of the device. Finite difference time domain simulation of electric field profile of the zipper cavity: (c) fundamental bonded mode with $\lambda = 1559$ nm, $Q_o = 1.8 \times 10^7$, and (d) fundamental anti-bonded mode with $\lambda = 1530$ nm, $Q_o = 9.2 \times 10^7$. (e) The torque sensing device (represented inside the yellow box) can be modeled as a coupled oscillator system where the nanodisk and readout nanobeam are mechanically coupled. The readout nanobeam forms one half of a photonic crystal zipper cavity. Motion of both the readout nanobeam and the auxiliary nanobeam of the cavity is optomechanically coupled to the cavity mode. Dynamics of each mode are described by the frequency ω and damping rate γ. Mechanical coupling between the nanodisk and readout nanobeam resonances is determined by g_M. The cavity optomechanical coupling is described by g_{OM}.

The coupled resonator system is illustrated in Fig. 1(a), and an example of a fabricated device is shown in Fig. 1(b). A suspended silicon nanodisk anchored to an unpatterned silicon-on-insulator (SOI) chip is connected to a photonic crystal nanobeam that forms one half of an optomechanical zipper cavity [30,31]. The second half of the zipper cavity is separated by a small gap from the coupled resonators and anchored to the unpatterned region of the chip; it is labeled as the auxiliary nanobeam in Fig. 1(b). The nanodisk can be mechanically driven by sources of torque (τ), for example, from nanomagnetic structures used in torque magnetometry [20,24,25], or by angular momentum transfer from structured optical fields [19]. Its design addresses limitations of previous photonic crystal torque sensors that detect cantilever-like motion of split-beam cavities [15], extending both the frequency range and nature of mechanical resonances that can be routinely measured. This is accomplished by resonantly coupling a wide spectrum of high-frequency mechanical resonances of the nanodisk to mechanical resonances of the zipper cavity. The zipper cavity combines high optical quality factor Q_o with large optomechanical coupling. It is formed following the fabrication process in Ref. [15]. The suspended photonic crystal nanobeams (width 500 nm, thickness 220 nm) are separated by a gap of 70 nm and patterned with holes of radius 110 nm. The hole spacing in each nanobeam tapers quadratically from $a_o = 400$ nm in the cavity's mirror region to $a_c = 350$ nm at the center of the cavity. The resulting cavity supports fundamental bonded and anti-bonded optical modes shown in Figs. 1(c) and 1(d), respectively, with predicted radiation loss limited $Q_o > 10^7$ in the 1500 nm wavelength band. Mechanical motion of the nanobeams can change the gap separating them, shifting the cavity mode frequencies. The frequency shift per unit displacement is quantified by optomechanical coupling coefficients $g^+_{OM}/2\pi \approx 85$ GHz/nm and $g^-_{OM}/2\pi \approx 2$ GHz/nm between the fundamental in-plane mechanical flexural resonance of the nanobeams and the bonded and anti-bonded optical cavity modes, respectively. The larger optomechanical coupling of the bonded mode arises from its higher field concentration in the gap, making it more susceptible to vibrations of the nanobeams. As a result, we focus on the bonded mode in this study.

In the absence of coupling between the nanodisk and the photonic crystal nanobeam, torque actuated motion of the nanodisk is not transduced by the cavity. However, transduction becomes possible when mechanical coupling is present. Intuitively, this transduction will be enhanced if the nanodisk motion is resonant with a nanobeam mode. This coupled oscillator approach to transduction of the "remote" and nominally dark nanodisk resonances is described by the model illustrated in Fig. 1(e). Motion of the readout nanobeam connected to the nanodisk is converted to an optical signal through its dispersive cavity optomechanical coupling quantified by g_{OM}. The dynamics of coupled nanodisk and readout nanobeam are described by equations of motion for the displacement amplitudes x_d and x_b of the nanodisk and readout nanobeam resonances, respectively:

$$\ddot{x}_d = -\omega_d'^2 x_d - \gamma_d \dot{x}_d + \sqrt{\frac{m_b}{m_d}} g_M^2 x_b + \frac{\tau_t}{I_d} f(t), \tag{1a}$$

$$\ddot{x}_b = -\omega_b'^2 x_b - \gamma_b \dot{x}_b + \sqrt{\frac{m_d}{m_b}} g_M^2 x_d, \tag{1b}$$

where ω_d, γ_d, m_d and ω_b, γ_b, m_b are the frequency, damping rate, and mass, respectively, of each uncoupled mechanical resonator. Note that $\omega_d' = \omega_d + \sqrt{\frac{m_b}{m_d}} g_M^2$ and $\omega_b' = \omega_b + \sqrt{\frac{m_d}{m_b}} g_M^2$ are the modified frequencies of the nanodisk and the readout nanobeam, respectively, when they are coupled. These equations include an external torsional drive $f(t)$ with an amplitude τ_t applied to the nanodisk, whose moment of inertia I_d is described by an effective mass m_{eff} and effective radius r_{eff} that is determined from the moment of inertia of the device, which relates the device's angular velocity to its energy, and is defined in [32]. Note that for generality an arbitrary drive is used here, where $f(t)$ is a real function. The mechanical susceptibilities $\chi_{d,b}(\omega) = (\omega_{d,b}'^2 - \omega^2 - i\gamma_{d,b}\omega)^{-1}$ and mechanical coupling g_M determine how effectively this applied torque is converted into motion of the readout nanobeam. The nanobeam amplitude can be derived by Fourier transforming Eqs. (1) and solving for x_b to obtain

$$x_b(\omega) = \frac{g_M^2}{\sqrt{\frac{m_b}{m_d}}((\chi_d(\omega)\chi_b(\omega))^{-1} - g_M^4)} \frac{\tau_t}{I_d} f(\omega). \tag{2}$$

Equation (2) shows that the resonantly driven transduced amplitude is enhanced,

$$|x_b(\omega_m)| = \frac{g_M^2}{\sqrt{\frac{m_b}{m_d}}(\gamma_d\gamma_b\omega_m^2 + g_M^4)}\frac{\tau_t}{I_d}, \quad (3)$$

when the nanodisk and readout nanobeam are resonant, i.e., $(\omega_d' = \omega_b' = \omega_m)$. Here, for simplicity, we have chosen the drive amplitude to be unity. The equation also implies that the mechanical mode frequencies become renormalized, as expected for a coupled system, with a frequency difference $\Delta\omega^2 \approx 2g_M^2$.

The coupling strength g_M depends on the device geometry and modes of interest. It can be determined by calculating the mode spectrum of the coupled resonators for varying device parameters such that the nanodisk and nanobeam modes are tuned through resonance. An example of this approach is shown in Fig. 2. We first show in Fig. 2(a) the mechanical frequencies of the individual components of the device for varying length l_s of the support beams anchoring the suspended nanodisk. We see that the nanobeam's in-plane flexural resonance frequencies remain constant, as expected since the nanobeam geometry is not affected by the support length, while the resonance frequencies of the nanodisk's in-plane twisting modes decrease quadratically with increasing l_s. In-plane twisting modes can be efficiently actuated by torque and for simplicity are referred to below as torsional modes.

At certain l_s values, the mechanical resonances of the uncoupled nanodisk and readout nanobeam are resonant and the resonance frequencies are renormalized by the mode coupling. This is shown in Fig. 2(b), which plots the full device's simulated mode spectrum for varying l_s. The anti-crossing behavior at points where the nanodisk and readout nanobeam modes are resonant is a signature of coupling between them. This mechanical coupling is the key feature that makes transduction of torsional actuation of the nanodisk to in-plane flexural motion of the readout nanobeam possible. Figure 2(c) shows g_M values extracted from the anti-crossing widths as a function of l_s for the first three harmonics of the nanodisk's twisting resonances. The trend of increasing g_M with increasing mechanical frequency suggests that higher frequency nanodisk resonances have better overlap with the nanobeam resonances at their clamping point. Similar increases in coupling between modes with increasing frequency are predicted when considering phononic clamping loss in nanomechanical resonators [33].

Optical detection of nanobeam displacement from torque applied to the nanodisk depends on the optomechanical coupling strength between the hybridized mode and the photonic crystal cavity, the mechanical mode compliance, and the mechanical coupling between the nanodisk and the nanobeam. To predict the efficacy of a given mode to optomechanically detect torque given all of these competing factors, we directly calculate the frequency shift of the cavity mode for a given torque. We achieve this by numerically calculating the mechanical displacement of the full device per unit applied external torque to the nanodisk, from which we then determine the resulting torsional optomechanical frequency shift $\Delta\omega_o \propto g_M^2 g_{OM}$. This shift, which captures both the device's cavity optomechanical coupling and the mechanical mode coupling, is shown by the color of the points in Fig. 2(d) for l_s swept through a typical anti-crossing. The simulated mechanical displacement profiles at several points within the anti-crossing are shown in Fig. 2(e). These simulated mechanical modes illustrate the evolution of the mode profiles across a mechanical anti-crossing region demonstrating the strong hybridization of the torsional modes at the center of the anti-crossing. This observation suggests that for torque sensing these strongly hybridized torsional modes are modes of interest. However, to effectively read out these modes, we require a significant nonzero displacement at the center of the nanobeam where the photonic crystal optical cavity is located. To illustrate that not all hybridized modes satisfy this criteria, we have added a gray dashed line to the center of the mode profiles (II) and (III) in Fig. 2(e). The lower frequency strongly hybridized mode has an anti-node at its center, which results in a stronger interaction with the optical cavity mode, leading to the optomechanical frequency shift $\Delta\omega_o$ and sensitivity being maximized at the center of the anti-crossing (II). And as we move away from this point towards modes (I) and (IV), we observe a decrease in $\Delta\omega_o$, as clearly suggested by their smaller amplitudes. On the other hand, the higher frequency strongly hybridized mode has a node at its center, which results in not only zero displacement at the cavity center, but an odd spatial symmetry of the displacement profile interacting with the cavity mode. This results in a weak interaction with the optical cavity mode, leading to a small $\Delta\omega_o$ and sensitivity at the center of the anti-crossing (III). More generally, for our cavity design, nanobeam modes with an even number of anti-nodes have small $\Delta\omega_o$ compared to modes with an odd number of anti-nodes.

2. RESULTS

To demonstrate the efficacy of the mode coupling effects discussed above, we experimentally study a range of devices with varying l_s. We optically measure the optomechanically transduced mechanical modes of our fabricated devices using a dimpled optical fiber taper waveguide [34] to evanescently couple light into and out of the cavity. Figure 3(a) shows the transmission profile of an optical cavity mode from a typical device. The measured mode has $Q_o \approx 160{,}000$ and a wavelength in the 1500 nm wavelength range. In a sideband unresolved system where the cavity field instantaneously follows the nanobeam's mechanical motion, the change in the cavity's optical intensity response from an applied torque is $\propto \tau(\omega_t)\Delta\omega_o dH/d\omega_L$. Here ω_L is the frequency of the probe laser input to the cavity, and $dH/d\omega_L$ is the slope of the cavity mode lineshape, where H is the normalized cavity transmission as a function of laser frequency. Due to the device's high sensitivity arising from its high-Q_o, large $\Delta\omega_o$, and low mass and associated large mechanical susceptibility [see Eq. (2)], thermomechanical driven motion of the mechanical resonances can be observed. Figure 3(b) shows a typical mechanical spectrum of a device ($l_s = 5.5$ μm).

A spectrum analyzer is used to convert the temporal fluctuations in fiber-taper transmission to a power spectral density. Peaks in the spectrum correspond to thermally driven motion of the nanobeam's mechanical resonances. Comparing the frequencies of the peaks in the spectrum with simulated values, we identified the hybridized torsional modes shown in Fig. 3(b) at frequencies that range from 6.3 to 784.6 MHz. Following the process in [15], one can extract the displacement resolution $\sqrt{S_{xx}}$ and torque sensitivity $\sqrt{S_{\tau\tau}}$ from these measurements as shown in Fig. 4. As the torque sensitivity $\sqrt{S_{\tau\tau}}$ in our system is limited by thermomechanical noise, it can be extracted from the thermomechanical displacement resolution $\sqrt{S_{xx}}$ by $\sqrt{S_{\tau\tau}} = \frac{m_{eff} r_{eff}}{|\chi_m(\omega)|}\sqrt{S_{xx}}$. This displacement resolution in our system can be calculated

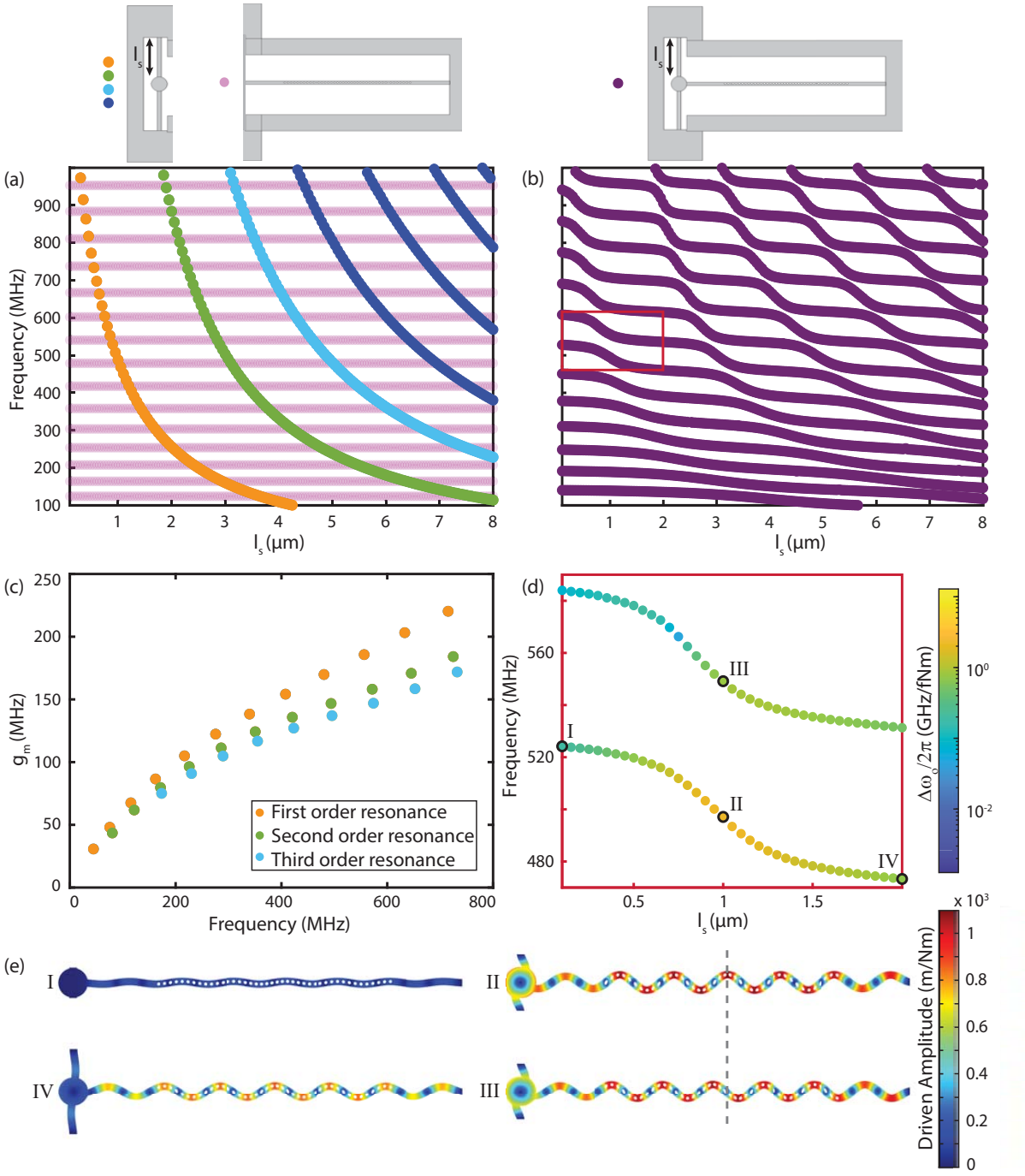

Fig. 2. (a) Individual simulated mechanical in-plane flexural resonances of uncoupled readout nanobeam (magenta) and torque actuated mechanical resonances of uncoupled nanodisk (orange, green, and cyan for first three resonances, respectively, and blue for remaining higher order resonances) as a function of the length of nanodisk's support beams l_s. (b) Simulated eigenfrequency of the in-plane hybridized torsional resonances of the device—coupled nanodisk and readout nanobeam—as a function of l_s. (c) Calculated mechanical coupling strengths g_M of a typical device for first three harmonics of nanodisk's resonances. (d) Zoom in of the region highlighted by a red box in (b) showing the calculated optomechanical frequency shift per unit applied torque as indicated by the color scale. (e) Displacement profiles of four mechanical resonances with different l_s, labeled I–IV in (d). The dashed gray line suggests the displacement profile at the center of the readout nanobeam, where the optical cavity is localized.

by measuring the signal-to-noise ratio (SNR) of the thermomechanically driven mechanical resonances using the expression $\sqrt{S_{xx}} = \sqrt{\frac{4k_B T Q_m / m_{eff}\omega_m^2}{(SNR)}}$, where k_B, T, and Q_m are the Boltzmann constant, temperature, and mechanical quality factor, respectively.

To analyze the torque sensitivity, we study three specific modes of interest, labeled [I–III] in the mechanical spectrum of the $l_s = 5.5$ μm device shown in Fig. 3(b), and plot them in Fig. 4. Based on the fits, we find a torque sensitivity range of $5.1 \times 10^{-21} - 1.2 \times 10^{-19}$ Nm/$\sqrt{\text{Hz}}$ depending on the mechanical mode. In particular, the weakly hybridized torsional mode with frequency 6.3 MHz, which is labeled [I] in Fig. 3(b), has the highest sensitivity value given above, while the hybridized torsional mode with frequency 784.6 MHz, which is labeled

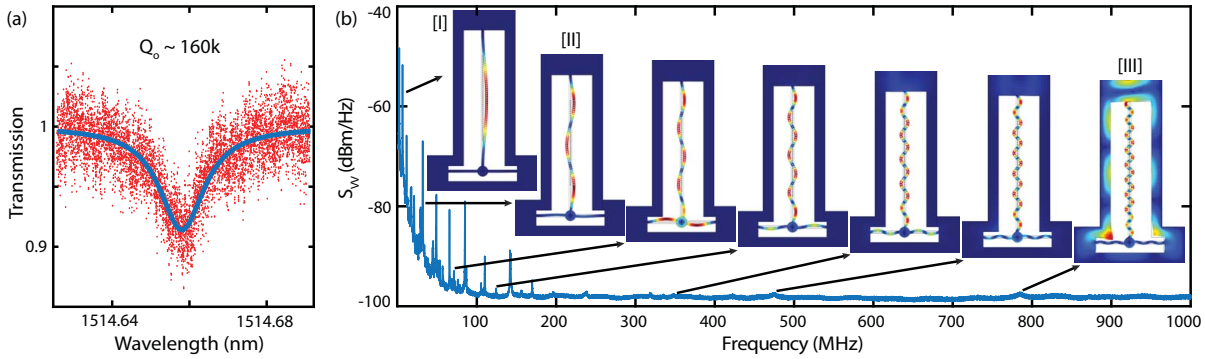

Fig. 3. (a) Measured optical transmission profile of the torque sensing device. (b) Optomechanical spectrum of the device in ambient conditions. Peaks correspond to thermally driven Brownian motion of the device's mechanical resonances. Peaks associated with torsional modes of the disk are identified. Three specific modes, labeled I–III, are chosen to demonstrate the torque sensitivity of this device, later in Fig. 4.

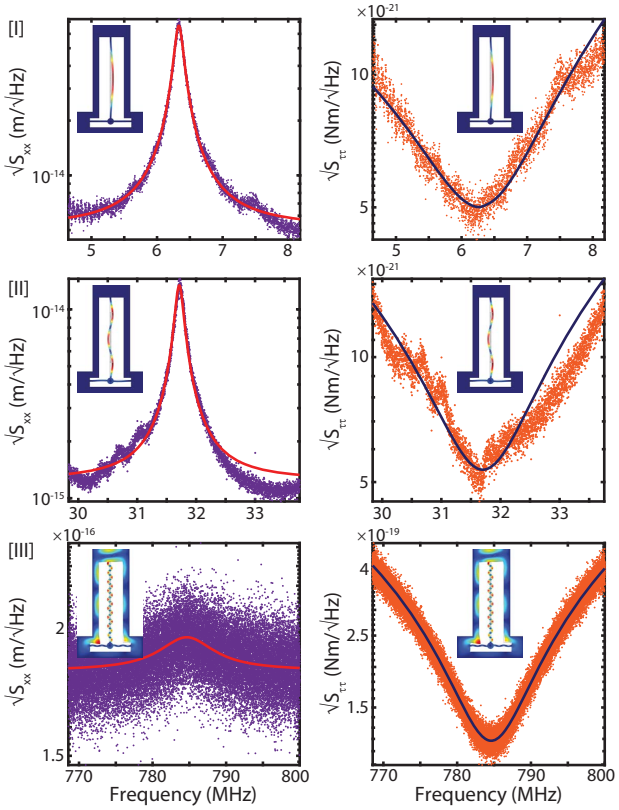

Fig. 4. Calculated displacement resolution $\sqrt{S_{xx}}$ and torque sensitivity $\sqrt{S_{\tau\tau}}$, and their respective fits—red solid line for displacement resolution and dark blue solid line for torque sensitivity—for the three specific modes of interest, labeled [I–III] in Fig. 3, of the device $l_s = 5.5$ μm.

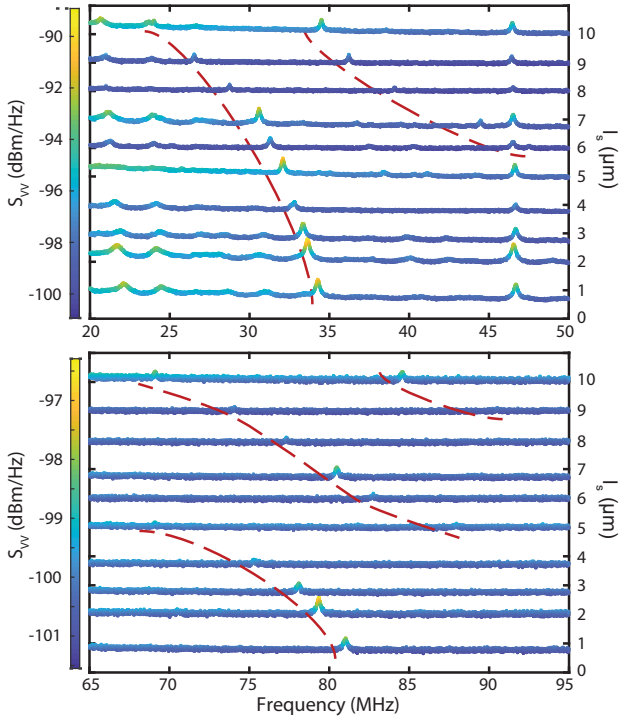

Fig. 5. Measured mechanical spectrum of the devices for varying support length. The signal strength is color coded. The red dashed line is a guide to the eye that follows the moving torsional peaks.

[III] in Fig. 3(b), is at the lower end of this sensitivity range. The strongly hybridized torsional mode with frequency 31.7 MHz, which is labeled [II] in Fig. 3(b), also has a high sensitivity value of 5.3×10^{-21} Nm/$\sqrt{\text{Hz}}$. Though mode [II] is more strongly hybridized than mode [I], because of relatively higher frequency and lower SNR, it has a slightly lesser torque sensitivity than that of mode [I]. Note that these measurements were made at room temperature and in ambient pressure. Operating in vacuum we expect the mechanical quality factors to increase, which will enhance the torque sensitivity [15]. Spectra were typically measured over an 83 s acquisition time. Further studies are required to determine how drift or other timescale dependent noise processes will impact the quoted sensitivities.

To further study the hybridization between the nanodisk and nanobeam resonances, the optomechanical spectrum was measured for devices with varying l_s. Figure 5 shows this measurement for l_s swept from 1 to 10 μm in increments of 1 μm. As shown by the red trend line, the torsional peaks shift with the expected anticrossing pattern predicted by the theory discussed in Figs. 2(a) and 2(b). Note that each measurement involves a unique device, and the contribution to the optical transduction related to the optical cavity mode and its coupling to the fiber taper will vary between devices.

To compare the measured results with theory more quantitatively, Fig. 6 plots the frequencies of the hybridized torsional resonances measured in Fig. 5 as a function of support length, together with the simulated values. The experimentally observed

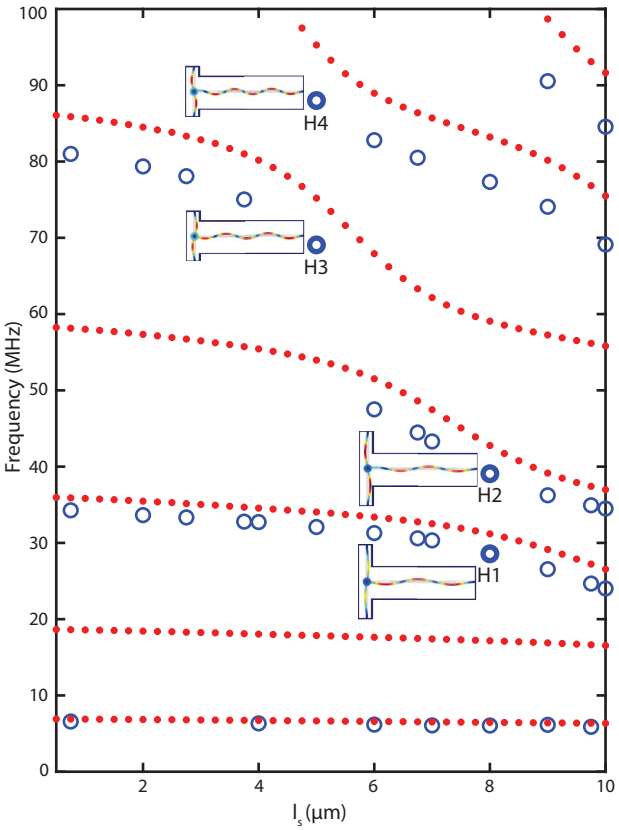

Fig. 6. Measured mechanical frequencies of the devices with varying support length (blue). The small red dots are simulated eigenfrequencies of the devices.

frequency dependence on support length is in good agreement with the simulated values, with variations most likely attributed to fabrication imperfections. Most crucially, the width of the observed anti-crossings closely match the predicted values. It is worth noting that peaks corresponding to nanobeam flexural resonances with an even number of anti-nodes do not appear in the spectrum. This can be understood from the fact that optomechanical couplings for these modes are near zero due to their odd symmetry around the center of the optical cavity.

3. CONCLUSION

The device demonstrated here shows how the high sensitivity of nanoscale optomechanical cavities can be harnessed to detect motion of nanomechanical resonators not integrated directly within the optical cavity. By coupling remote and optically dark mechanical resonances to resonators integrated within a photonic crystal nanocavity, mechanical resonances with a wide range of frequencies, mode profiles, and symmetries can be sensitively transduced. Since the nanomechanical resonator does not interact directly with the cavity field, it can be decorated with optically lossy metals or magnetic materials. This is of particular interest for advancing the performance and frequency range of optomechanical torque magnetometers used to probe the nanomagnetic properties of permalloy [20]. To this end, the device has demonstrated torque sensitivity of $5.1 \times 10^{-21} - 1.2 \times 10^{-19}$ Nm/$\sqrt{\text{Hz}}$ for a mechanical frequency range of 5–800 MHz. Previous nanoscale cavity optomechanical torque sensing devices [15,18,22] achieve similar or better sensitivities, but are limited to frequencies below 20 MHz. To the best of our knowledge, the current state-of-the-art in torque sensitivity in an on-chip platform is $\sim 10^{-24}$ Nm/$\sqrt{\text{Hz}}$ at cryogenic temperatures in the <20 MHz mechanical frequency range [22], while the current state-of-the-art in a levitated nanoparticle in vacuum platform is $\sim 10^{-27}$ Nm/$\sqrt{\text{Hz}}$ at room temperature with a rotation frequency >5 GHz [35]. The sensitivity of our devices can be further improved by orders of magnitude by performing the experiment in ultrahigh vacuum and cryogenic temperatures where mechanical quality factors in silicon devices can reach $Q_m > 10^8$ [36]. Operation at higher (>GHz) frequencies may be possible using this approach by combining torque actuated mechanical resonators with optomechanical crystal cavities and waveguides [37].

In the near future, the device's ability to operate at frequencies >100 MHz will enable high-frequency torque magnetometry studies of nanomagnetic systems, opening the door to observation of the Einstein–de Haas effect [25,26], as well as resonant coupling between nanomagnetic spin dynamics and the optomechanical system. Signatures of the Einstein–de Hass effect in driven magnetic spin-mechanical systems become more pronounced at high frequencies [26]. Studies of magnetic resonances typically occur at frequencies above 100 MHz, and one needs to be at a similar or higher mechanical detection bandwidth to study their magnetization dynamics. In cases where the detection bandwidth is much narrower than the rate of angular momentum transfer between the magnetic and mechanical system, the ability to detect a torque will give insight into spin-lattice relaxation processes, which are of fundamental importance to condensed matter physics research. Furthermore, with the integration of the torsional device with magnetic materials it will also become possible to generate effective couplings between light and magnetic spins, with applications in the development of hybrid quantum systems [38].

Funding. Natural Sciences and Engineering Research Council of Canada (Discovery Grant, Strategic Partnership Grant programs); Alberta Innovates—Technology Futures (Strategic Research Project program); Canadian Foundation for Innovation; National Research Council Canada (Nanotechnology Initiative).

Acknowledgment. The authors acknowledge helpful discussion with M. Mitchell, P. Parsa, D. Sukachev, M. Freeman, and J. Losby.

Disclosures. The authors declare no conflicts of interest.

Data availability. Data underlying the results presented in this paper are not publicly available at this time but may be obtained from the authors upon reasonable request.

†These authors contributed equally to this paper.

REFERENCES

1. M. Aspelmeyer, T. J. Kippenberg, and F. Marquardt, "Cavity optomechanics," Rev. Mod. Phys. **86**, 1391–1452 (2014).
2. J. Xia, Q. Qiao, G. Zhou, F. S. Chau, and G. Zhou, "Opto-mechanical photonic crystal cavities for sensing application," Appl. Sci. **10**, 7080 (2020).
3. X. Sun, J. Zhang, M. Poot, C. Wong, and H. Tang, "Femtogram doubly clamped nanomechanical resonators embedded in a high-Q two-dimensional photonic crystal nanocavity," Nano Lett. **12**, 2299–2305 (2012).
4. E. Gavartin, P. Verlot, and T. Kippenberg, "A hybrid on-chip optomechanical transducer for ultrasensitive force measurements," Nat. Nanotechnol. **7**, 509–514 (2012).
5. J. Gomis-Bresco, D. Navarro-Urrios, M. Oudich, S. El-Jallal, A. Griol, D. Puerto, E. Chavez, Y. Pennec, B. Djafari-Rouhani, F. Alzina, A. Martínez,

and C. M. Sotomayor Torres, "A one-dimensional optomechanical crystal with a complete phononic band gap," Nat. Commun. **5**, 4452 (2014).
6. C. P. Ho, P. Pitchappa, B. W. Soon, and C. Lee, "Suspended 2-d photonic crystal aluminum nitride membrane reflector," Opt. Express **23**, 10598–10603 (2015).
7. K. Han, K. Zhu, and G. Bahl, "Opto-mechano-fluidic viscometer," Appl. Phys. Lett. **105**, 014103 (2014).
8. B.-B. Li, L. Ou, Y. Lei, and Y.-C. Liu, "Cavity optomechanical sensing," Nanophotonics **10**, 2799–2832 (2021).
9. X. Liu, W. Liu, Z. Ren, Y. Ma, B. Dong, G. Zhou, and C. Lee, "Progress of optomechanical micro/nano sensors: a review," Int. J. Optomech. **15**, 120–159 (2021).
10. A. G. Krause, M. Winger, T. D. Blasius, W. Lin, and O. Painter, "A high-resolution microchip optomechanical accelerometer," Nat. Photonics **6**, 768–772 (2012).
11. S. Basiri-Esfahani, A. Armin, S. Forstner, and W. P. Bowen, "Precision ultrasound sensing on a chip," Nat. Commun. **10**, 132 (2019).
12. M. Sansa, M. Defoort, A. Brenac, M. Hermouet, L. Banniard, A. Fafin, M. Gely, C. Masselon, I. Favero, G. Jourdan, and S. Hentz, "Optomechanical mass spectrometry," Nat. Commun. **11**, 3781 (2020).
13. J.-J. Li and K.-D. Zhu, "Nonlinear optical mass sensor with an optomechanical microresonator," Appl. Phys. Lett. **101**, 141905 (2012).
14. Y. Liu, H. Miao, V. Aksyuk, and K. Srinivasan, "Wide cantilever stiffness range cavity optomechanical sensors for atomic force microscopy," Opt. Express **20**, 18268–18280 (2012).
15. M. Wu, A. C. Hryciw, C. Healey, D. P. Lake, H. Jayakumar, M. R. Freeman, J. P. Davis, and P. E. Barclay, "Dissipative and dispersive optomechanics in a nanocavity torque sensor," Phys. Rev. X **4**, 021052 (2014).
16. J. G. Huang, H. Cai, Y. Gu, L. Chin, J. Wu, T. Chen, Z. Yang, Y. Hao, and A. Liu, "Torsional frequency mixing and sensing in optomechanical resonators," Appl. Phys. Lett. **111**, 111102 (2017).
17. L. He, H. Li, and M. Li, "Optomechanical measurement of photon spin angular momentum and optical torque in integrated photonic devices," Sci. Adv. **2**, e1600485 (2016).
18. P. Kim, C. Doolin, B. Hauer, A. MacDonald, M. Freeman, P. Barclay, and J. Davis, "Nanoscale torsional optomechanics," Appl. Phys. Lett. **102**, 053102 (2013).
19. H. Kaviani, R. Ghobadi, B. Behera, M. Wu, A. Hryciw, S. Vo, D. Fattal, and P. Barclay, "Optomechanical detection of light with orbital angular momentum," Opt. Express **28**, 15482–15496 (2020).
20. M. Wu, N. L.-Y. Wu, T. Firdous, F. F. Sani, J. E. Losby, M. R. Freeman, and P. E. Barclay, "Nanocavity optomechanical torque magnetometry and radiofrequency susceptometry," Nat. Nanotechnol. **12**, 127 (2017).
21. P. Kim, B. Hauer, T. Clark, F. F. Sani, M. Freeman, and J. Davis, "Magnetic actuation and feedback cooling of a cavity optomechanical torque sensor," Nat. Commun. **8**, 1355 (2017).
22. P. Kim, B. Hauer, C. Doolin, F. Souris, and J. Davis, "Approaching the standard quantum limit of mechanical torque sensing," Nat. Commun. **7**, 13165 (2016).
23. W. Jiang, C. J. Sarabalis, Y. D. Dahmani, R. N. Patel, F. M. Mayor, T. P. McKenna, R. Van Laer, and A. H. Safavi-Naeini, "Efficient bidirectional piezo-optomechanical transduction between microwave and optical frequency," Nat. Commun. **11**, 1166 (2020).
24. G. Hajisalem, J. E. Losby, G. de Oliveira Luiz, V. T. Sauer, P. E. Barclay, and M. R. Freeman, "Two-axis cavity optomechanical torque characterization of magnetic microstructures," New J. Phys. **21**, 095005 (2019).
25. J. E. Losby, V. T. Sauer, and M. R. Freeman, "Recent advances in mechanical torque studies of small-scale magnetism," J. Phys. D **51**, 483001 (2018).
26. K. Mori, M. Dunsmore, J. Losby, D. Jenson, M. Belov, and M. Freeman, "Einstein–de Haas effect at radio frequencies in and near magnetic equilibrium," Phys. Rev. B **102**, 054415 (2020).
27. T. Delord, P. Huillery, L. Nicolas, and G. Hétet, "Spin-cooling of the motion of a trapped diamond," Nature **580**, 56–59 (2020).
28. T. Bagci, A. Simonsen, S. Schmid, L. G. Villanueva, E. Zeuthen, J. Appel, J. M. Taylor, A. Sørensen, K. Usami, A. Schliesser, and E. S. Polzik, "Optical detection of radio waves through a nanomechanical transducer," Nature **507**, 81–85 (2014).
29. A. Pearson, K. Khosla, M. Mergenthaler, G. A. D. Briggs, E. Laird, and N. Ares, "Radio-frequency optomechanical characterization of a silicon nitride drum," Sci. Rep. **10**, 1654 (2020).
30. J. Chan, M. Eichenfield, R. Camacho, and O. Painter, "Optical and mechanical design of a "zipper" photonic crystal optomechanical cavity," Opt. Express **17**, 3802–3817 (2009).
31. M. Eichenfield, R. Camacho, J. Chan, K. J. Vahala, and O. Painter, "A picogram and nanometer scale photonic crystal opto-mechanical cavity," Nature **459**, 550–555 (2009).
32. B. Hauer, C. Doolin, K. Beach, and J. Davis, "A general procedure for thermomechanical calibration of nano/micro-mechanical resonators," Ann. Phys. **339**, 181–207 (2013).
33. I. Wilson-Rae, "Intrinsic dissipation in nanomechanical resonators due to phonon tunneling," Phys. Rev. B **77**, 245418 (2008).
34. C. P. Michael, M. Borselli, T. J. Johnson, C. Chrystala, and O. Painter, "An optical fiber-taper probe for wafer-scale microphotonic device characterization," Opt. Express **15**, 4745–4752 (2007).
35. J. Ahn, Z. Xu, J. Bang, P. Ju, X. Gao, and T. Li, "Ultrasensitive torque detection with an optically levitated nanorotor," Nat. Nanotechnol. **15**, 89–93 (2020).
36. G. S. MacCabe, H. Ren, J. Luo, J. D. Cohen, H. Zhou, A. Sipahigil, M. Mirhosseini, and O. Painter, "Nano-acoustic resonator with ultralong phonon lifetime," Science **370**, 840–843 (2020).
37. K. Fang, J. Luo, A. Metelmann, M. H. Matheny, F. Marquardt, A. A. Clerk, and O. Painter, "Generalized non-reciprocity in an optomechanical circuit via synthetic magnetism and reservoir engineering," Nat. Phys. **13**, 465–471 (2017).
38. M. Wallquist, K. Hammerer, P. Rabl, M. Lukin, and P. Zoller, "Hybrid quantum devices and quantum engineering," Phys. Scr. **T137**, 014001 (2009).